ORIGINAL RESEARCH

Arteriovenous Shunt Visualization in Arteriovenous Malformations with Arterial Spin-Labeling MR Imaging

R.L. Wolf
J. Wang
J.A. Detre
E.L. Zager
R.W. Hurst

BACKGROUND AND PURPOSE: A reliable quantitative technique for measuring arteriovenous (AV) shunt in vascular malformations is not currently available. Here, we evaluated the hypothesis that continuous arterial spin-labeled (CASL) perfusion MR imaging can be used to detect and measure AV shunt in patients with arteriovenous malformations (AVMs).

MATERIALS AND METHODS: CASL perfusion MR imaging was performed in 7 patients with AVMs. Semiquantitative AV shunt estimates were generated based on a thresholding strategy by using signal-intensity difference (ΔM) images to avoid potential errors in cerebral blood flow (CBF) calculation related to abnormal transit times and nonphysiologic blood-tissue water exchange in and around the AVMs. The potential for measuring CBF in regions distant from and near the AVM was explored, as was the relationship of CBF changes related to the size of the shunt.

RESULTS: In all 7 cases, striking increased intensity was seen on CASL perfusion ΔM maps in the nidus and venous structures draining the AVM. Shunt estimates ranged from 30% to 0.6%. Mean CBF measurements in structures near the AVMs were not significantly different from the contralateral measurements. However, CBF in adjacent ipsilateral white matter increased relative to the contralateral side as the percent shunt increased ($P = .02$). Cortical gray matter CBF Δ (contralateral-ipsilateral) values demonstrated the same effect, but the correlation was weak and not significant. Thalamic CBF decreased ipsilaterally with increasing percent AV shunt ($P = .01$), indicating a possible steal effect. Basal ganglia Δ values showed little change in CBF with the size of the AV shunt.

CONCLUSION: CASL perfusion MR imaging can demonstrate AV shunting, providing high lesion conspicuity and a novel means for evaluating AVM physiology.

Arteriovenous malformations (AVMs) are congenital abnormalities in vascular development in which arteriovenous (AV) shunting is present. Symptoms may be acute or chronic, but the presenting event in 40%–70% of patients with AVMs is intracranial hemorrhage,[1-3] with potentially significant morbidity and mortality. MR imaging and CT techniques can be used for evaluation of AVMs, but the vascular architecture and hemodynamics of AVMs are often complex, and the gold standard for evaluation is conventional digital subtraction angiography (DSA). Dural arteriovenous fistulas (DAVFs) represent another type of AVM and can be acquired, perhaps developing after venous sinus occlusion or trauma. Direct arteriovenous connections are present without a nidus, so these can be difficult to detect and localize even with DSA.

MR angiography (MRA) techniques provide a noninvasive alternative for evaluating AVMs; however, the spatial and temporal resolution of DSA is not currently available. Although submillimeter spatial resolution is possible in all 3 planes and methods exist with temporal resolution of <1 second,[4] it is difficult to obtain high temporal and spatial resolution in the same acquisition (and in 3D). Phase-contrast MR imaging has been used to measure blood flow in arteries feeding AVMs, but it is not adequate for comprehensive evaluation of AVM hemodynamics or effects on adjacent brain.[5,6] Undersampled back projection and keyhole imaging approaches and also parallel imaging methods[7-12] may provide the means for a favorable comparison with DSA to the point where it is possible to obtain complete evaluation of AVM vascular architecture as well as dynamic characteristics, including AV shunting and blood flow in adjacent brain, but current noninvasive imaging methods remain suboptimal. Even DSA is not capable of providing accurate quantitative assessment of blood flow or degree of shunt in an AVM, though there are objective indirect measures such as venous appearance time.

In arterial spin-labeled (ASL) perfusion MR imaging studies of the brain, arterial blood water is used as an endogenous tracer, typically with a pulsed or continuous labeling approach. A delay allows arterial blood flow into the imaging plane, during which time there is T1 decay of the label. Subtraction of labeled images from unlabeled control images yields a difference image, in which measured signal-intensity change is proportional to cerebral blood flow (CBF). Although labeled arterial blood water is nominally a diffusible tracer, T1 relaxation is relatively short compared with transit time, and most labeled blood will relax during transit through capillaries, before exchange with brain tissue water.[13-16] Because microvessels are small compared with voxel size, the tracer distribution is comparable to what would be observed if it had diffused into tissue.

Transit effects present technical challenges in measuring

Received August 16, 2007; accepted after revision October 18.

From the Departments of Radiology (R.L.W., J.W., J.A.D., R.W.H.), Neurology (J.W., J.A.D.), and Neurosurgery (E.L.Z., R.W.H.), University of Pennsylvania Medical Center, Philadelphia, Pa.

This work was partially supported by National Institutes of Health grants RR002305 (J.A.D, J.W.), NS045839 (J.A.D.), and K23 NS043381 (R.L.W.). J.A. Detre is named on a patent for ASL.

Paper previously presented in part at: Annual Meeting of the International Society for Magnetic Resonance in Medicine, May 6–12, 2006; Miami, Fla.

Please address correspondence to Ronald L. Wolf, MD, PhD, University of Pennsylvania Medical Center, Department of Radiology, Section of Neuroradiology, Dulles 219, 3400 Spruce St, Philadelphia, PA 19104; e-mail: Ronald.Wolf@uphs.upenn.edu

DOI 10.3174/ajnr.A0901

CBF with ASL methods.[17,18] Consolidation of label in a vascular compartment occupying more than approximately 5% (approximate normal cerebral blood volume in gray matter) of a voxel would appear as high signal intensity. When there is a transit delay due to stenotic-occlusive disease, substantial label is still in larger arteries (macrovessels) supplying the brain, thus appearing as intraluminal hyperintensities. In a normal human brain, there is minimal venous outflow of label; however, in AVMs, there is abnormal shortening of transit time. Labeled blood flowing through an AVM no longer behaves as a microvascular tracer because a normal capillary bed is not present, instead behaving as a macrovascular or intraluminal tracer. The effect is analogous to MRA using ASL,[19-22] where an AVM nidus and draining veins may appear as high-contrast structures with a macrovascular label representing rapid transit (AV shunting). However, in theory, CBF can still be evaluated in the rest of the brain where label has been delivered to microvasculature of normal brain tissue.

The purpose of this work was to investigate the hypothesis that ASL perfusion methodology can be applied to detect and quantify rapid transit through an AVM, which can potentially be exploited for detection of AVMs and perhaps quantification of AV shunting longitudinally and following treatment. Secondary goals were to determine whether plausible values for CBF (ie, within expected limits of published values) could be obtained in regions of the brain adjacent to or distant from the AVM and, if so, whether detectable differences were present.

Methods

Subjects

Subjects were 7 patients (mean age, 41; range, 23–65) with AVMs in whom continuous ASL (CASL) MR perfusion imaging studies were performed as part of functional MR imaging examinations clinically requested for preoperative planning. AVMs were confirmed on DSA, 5 performed at our institution and 2 performed at outside institutions (AVM findings confirmed by reports from the latter 2 outside studies). For comparison, CASL perfusion data from 2 patients (ages 32 and 60) with cavernous angioma (which should not demonstrate AV shunt) and 10 patients with glioblastoma (which could potentially demonstrate AV shunting) were also reviewed (mean age, 54.1; range, 43–74). Data were acquired within the guidelines of the local institutional review board, and written consent was obtained.

MR Imaging

All studies were performed on a 3T Magnetom Trio (Siemens, Erlangen, Germany) whole-body scanner by using a product transmit/receive head coil. Structural imaging in all patients included a 3D T1-weighted sequence (magnetization-preparation rapid acquisition of gradient echo), fluid-attenuated inversion recovery, and, in 6/7 subjects, 2D or 3D time-of-flight (TOF) MRA of the AVM. The remaining subject had only a conventional DSA for comparison.

Parameters for CASL perfusion MR imaging included TR/TE = 4000/17 ms, matrix = 64 × 64, number of sections = 12–16, section thickness = 6 mm (1.5-mm gap), labeling delay = 1200 ms, and FOV = 22 × 22 cm^2. Total acquisition time was 5:28 minutes. One patient was studied after 2 prior partial embolizations, by using delay times of both 800 and 1200 ms. The last embolization had been performed 8 days before CASL perfusion MR imaging. We studied another patient before and 2 days after embolization, obtaining CASL perfusion MR imaging at delay times ranging from 200 to 1500 ms during the postoperative study (only 1 acquisition at 1200 ms was obtained before embolization). In all cases, a reduced radio-frequency amplitude of labeling pulses (2.25 μT) and a weaker 1.6 mT/m labeling gradient were used to remain within US Food and Drug Administration guidelines for radio-frequency deposition at 3T. Labeling and sinusoidal control pulses (100 Hz) were applied at the cervicomedullary junction. All perfusion images were spatially smoothed by using a 2D gaussian kernel with a full width at half maximum of 0.7 mm.

Image Analysis

The signal intensity difference (ΔM) image was sufficient to evaluate the presence of AV shunting and was used primarily to avoid potential errors in CBF calculation related to abnormal transit times and potential nonphysiologic blood-tissue-water exchange in and around AVMs. A semiquantitative approximation of the degree of shunting was first explored on the basis of a simple threshold as follows: 1) a standardized 13-voxel region of interest was placed in the contralateral basal ganglia (BG), and mean (BG_{mean}) and SD (BG_{SD}) were measured for each patient with AVM; 2) voxels with intensity greater than an empirically chosen threshold of $BG_{mean} + 8 * BG_{SD}$ were automatically selected to create a mask for AVM and shunt vessels; 3) an estimate of the fraction of labeled blood shunted through the AVM was generated by multiplying mean ΔM in masked voxels by the number of voxels and dividing by the mean ΔM in the entire brain multiplied by all labeled voxels (Fig 1). For this approach, the labeled blood water can be simply viewed as a blood pool tracer (ie, a 1-compartment model), where label is in the microvasculature for the brain and in the macrovasculature for the AVM. The automatically segmented AVM mask was compared with MRA and DSA images when available to confirm reasonable selection of voxels within the AVM and draining vessels. At the same time, available DSA studies were reviewed by 2 experienced neuroradiologists (R.L.W. and R.W.H., with R.W.H. also an experienced neurointerventionalist) for feeding vessels, venous appearance time, and draining vessels.

The potential for measuring CBF in regions distant from and, if possible, near the AVM was also explored. To this end, CBF was calculated as described in the equation:

$$CBF = \frac{\lambda \Delta M R_{1a}}{2\alpha M_{control}\{\exp(-wR_{1a}) - \exp[-(\tau + w)R_{1a}]\}},$$

where α is labeling efficiency, λ is the water fraction of arterial blood (0.9), R_{1a} is the longitudinal relaxation rate of blood ($R_{1a} = 1/T_{1a}$, with T_{1a} assumed to be constant at 1490 ms for this study),[23] ΔM is the difference between control and labeled image intensities, $M_{control}$ is the average control image intensity, τ is the labeling pulse duration, and w is the postlabeling delay time.[24-26] Use of a fixed T_{1a} rather than measuring tissue T_1 assumes that the labeled spins remain primarily in the microvasculature rather than exchanging completely with tissue water.[13-16] This assumption is particularly valid in patients with cerebrovascular disease in whom arterial transit times are prolonged but may not be tenable for rapid arterial transit times, so that CBF calculations were not attempted for voxels likely to contain shunt label.

Small standardized regions of interest (13 voxels) were placed by 1 investigator (R.L.W.) in the basal ganglia and thalamus bilaterally, and mean CBF and raw signal intensity were calculated. Similar regions of interest were placed in the white matter and cortex immediately anterior and posterior to the AVM but avoiding large-vessel or

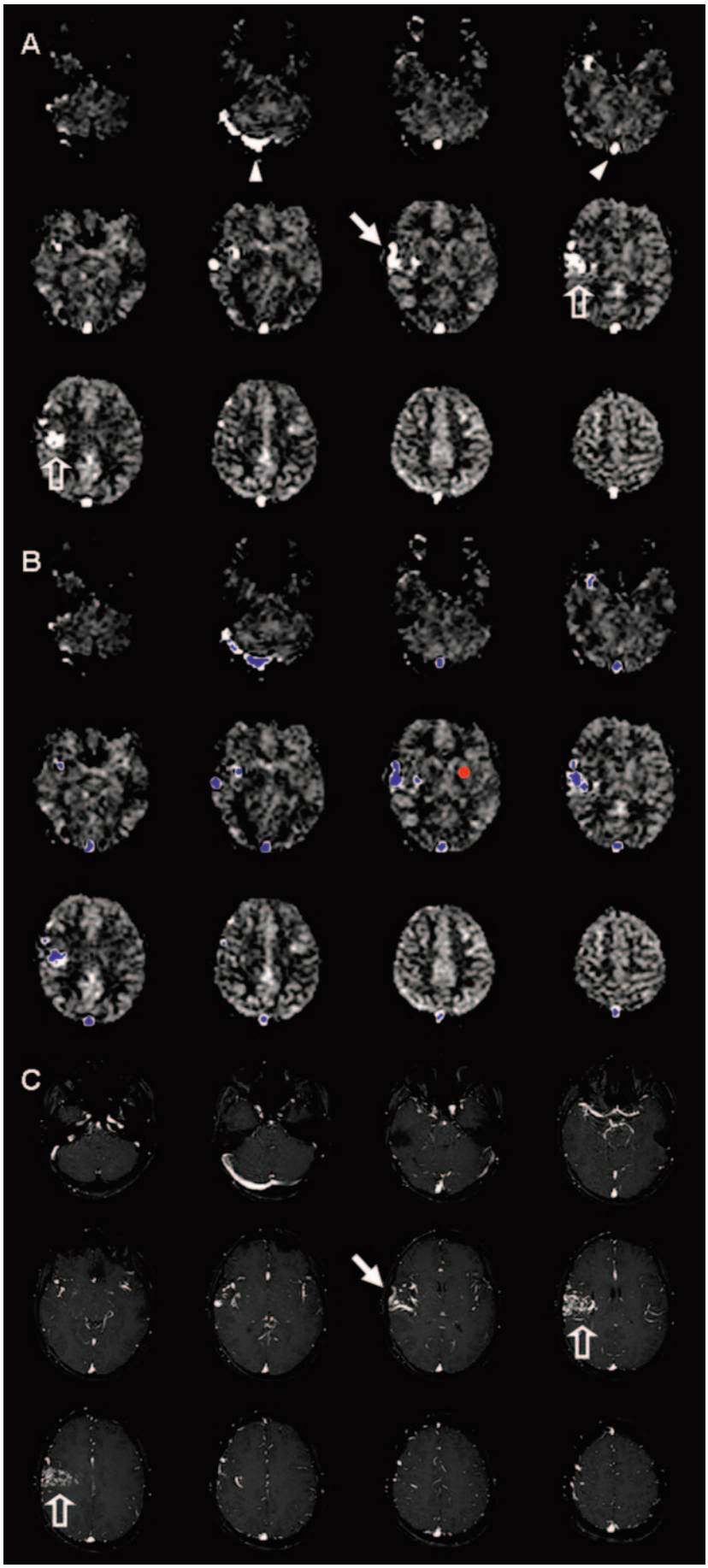

Fig 1. Image evaluation and shunt approximation for a right hemisphere AVM. *A,* CASL perfusion ΔM maps show bright signal intensity in the sagittal sinus and right transverse sinus (*arrowheads*) and in draining veins (*arrows*) adjacent to the nidus (*open arrows*). *B,* A small region of interest (*red circle*) placed in the left basal ganglia is used for each patient to measure mean ΔM (BG_{mean}) and SD (BG_{SD}). A threshold is generated (empirically chosen as threshold = BG_{mean} + 8 *BG_{SD}) above which voxels are labeled as shunt voxels to create a mask (blue voxels) for the AVM and draining vessels. The AV shunt fraction is estimated by multiplying the mean ΔM in the mask by the number of voxels in the mask, then dividing by the mean ΔM in the entire brain multiplied by all labeled voxels. *C,* Registered 2D TOF MRA source images (no superior saturation band) are reviewed to verify reasonable selection of AVM and draining vessels (*open and closed arrows*).

shunt signal-intensity pixels. Anterior and posterior white matter and cortical regions of interest were averaged. Mirror regions of interest were chosen in the contralateral hemisphere. Δ values were calculated by subtracting mean values in ipsilateral regions of interest from contralateral regions of interest. Positive values thus indicated hypoperfusion on the side of the AVM, and negative values indicated hyperperfusion. For the patient studied after prior partial embolizations, perfusion data were acquired 8 days after the most recent embolization. This was believed to be sufficient for CBF to have stabilized. For the patient studied before and after embolization, only perfusion data acquired before embolization were included in the analysis.

Statistical Analysis

Statistics were generated using JMP 4.0 software (SAS Institute, Cary, NC), by using paired *t* tests for comparisons of ipsilateral versus contralateral CBF or raw signal intensity in sampled regions and linear regression for describing relationships between perfusion values and percent AV shunt.

Results

Clinical data and AVM features are detailed in Table 1. The Spetzler-Martin grade[1] ranged from 2 to 4, with all AVMs receiving a dominant supply from anterior circulation vessels. Venous arrival times relative to the supraclinoid internal carotid artery ranged from 0.27 to 0.67 seconds. Contrast arrival time in normal venous structures was between 3 and 4 seconds for 4 of 5 subjects in whom DSA studies were available, but just over 6 seconds in 1 subject with the largest AVM and the only AVM with deep venous drainage (patient 7). In all 7 patients, striking increased intensity was seen on CASL perfusion ΔM maps in venous structures draining the AVM. Typical findings for 1 of the patients with AVM (patient 6) are shown in Fig 1. Approximations of percent AV shunt ranged from 30% for the largest AVM to 0.6% for the smallest (Table 2). One of the patients with glioblastoma showed apparent

Table 1: Clinical data and AVM features

Patient	Age (yr)	Presentation	Location	Eloquent Tissue at Risk	Grade (size/ eloquent/ drainage)*	Arterial Supply	VAT AVM/normal (s)
1	65	Headache	Left frontal	Broca area	2/1/0	L M2–3, L ACA	0.67/3.87
2	44	Bleed + seizures	Right frontal-parietal	Primary sensorimotor cortex	2/1/0	R M3–4	0.54/3.74
3	23	Hand/Face numbness	Left frontal-parietal	Primary sensorimotor cortex	1/1/0	L M4	0.27/3.87
4	33	Bleed + headache, expressive dysphasia	Left frontal	Broca area	1/1/0	L M4	NA
5	49	Headache	Left occipital-temporal	Visual cortex, optic radiations	1/1/0	L M4	NA
6	23	Left face/tongue spasms	Right frontal-parietal	Primary sensorimotor cortex	2/1/0	R M3–4	0.4/3.2
7	47	Headache, blurry vision	Left frontal	Broca area	2/1/1	L M1–4, L ACA	0.53/6.13

Note:—VAT indicates venous appearance time with contrast appearance in supraclinoid artery as reference point (t = 0 seconds) for both AVM and normal venous structures; NA, not available (DSA performed elsewhere); R, right; L, left; M1–4, middle cerebral artery branches; ACA, anterior cerebral artery.
* Spetzler-Martin grade by category (size, involvement of eloquent brain, and drainage pattern) with eloquent regions defined as primary sensorimotor cortex, language and visual cortex, hypothalamus and thalamus, internal capsule, brain stem, and deep cerebellar nuclei.[1]

Table 2: AVM data and CBF comparisons ipsilateral and contralateral to AVM

			CBF (mL/100 g/min)								
Patient	Grade*	Shunt (%)	CBF_{mean}	BG_{ips}	BG_{cont}	$Thal_{ips}$	$Thal_{cont}$	GM_{ips}	GM_{cont}	WM_{ips}	WM_{cont}
1	3	23.42	50.7	49.6	37.8	51.2	53.9	61.7	58.9	29.8	23.8
2	3	19.80	54.7	44.3	47	66.8	76.6	85.9	53.3	25.4	15.5
3	2	4.90	52.3	39.0	49.0	45.8	42.9	67.3	78.6	13.6	16.1
4	2	0.64	61.3	67.8	63.6	66.6	48.5	84.5	88.2	23.8	34.4
5	2	3.13	39.0	35.0	36.7	48.4	45.1	49.7	37.1	17.4	22.2
6	3	10.72	39.7	39.3	41.4	36.0	40.1	48.0	62.8	21.6	25.0
7	4	29.74	48.2	34.6	44.7	42.6	58.6	62.3	51.2	39.7	35.8
Mean			49.4	44.3	45.7	51.1	52.2	65.6	61.5	24.5	24.7

Note:—CBF_{mean} indicates mean brain cerebral blood flow excluding AVM and associated structures; GM (WM), gray matter (white matter) blood flow averaged from regions of interest anterior and posterior to the AVM; Thal, thalamus; ips, ipsilateral; cont, contralateral.
* Grade indicates total Spetzler-Martin grade (sum of scores for size, involvement of eloquent brain, and drainage pattern as listed in Table 1).

AV shunting in the sagittal sinus, with the glioblastoma in this case fairly large (5 cm) and peripherally located in the parietal lobe adjacent to the sagittal sinus. The calculated shunt fraction in this case was 0.48%. None of the other comparison patients demonstrated this effect (calculated mean shunt fraction, 0.12%; range, 0%–0.48%). For the 2 patients with cavernous angiomas, no shunt was demonstrated on visual inspection, and the calculated shunt fraction was 0%.

Figure 2 demonstrates changes after partial embolization of a large left frontal AVM. Shunt estimates decreased from 23% before embolization to 20% after embolization of 1 feeding pedicle (using Onyx Liquid Embolic System; MicroTherapeutics, Irvine, Calif). The interventionalist estimated a reduction in AVM blood flow of approximately 20%, which would translate roughly to just under a 5% decrease in AV shunt fraction (concordant with the 3% measured decrease). This comparison is only speculative, however, because the error in measurement of AV shunt fraction with this technique is not known and cannot be generated with existing data. Interpretation is complicated by the presence of embolic material, thrombus, and/or hemorrhage because signal-intensity dropout occurs on source images (Fig 3). Presumably, these regions will not have blood flow and should not substantially alter the estimate of shunt because they do not contribute to the calculation. However, signal-intensity loss adjacent to areas of artifact could lead to underestimation of the extent of shunt in some voxels. In this case, evidence of AV shunting was still detected despite foci of signal intensity loss. This is relevant to the patients with cavernous angioma, in whom susceptibility artifact will often be present and preclude accurate measurement of blood flow in and immediately adjacent to the cavernous angioma. However, this would not prevent detection of label in draining venous structures, which would allow distinction between small AVMs with hemorrhage and cavernous angiomas. For patients 2 and 7, as well as patient 1 (above, Fig 2), intense signal intensity on CASL perfusion images corresponded to very small draining veins on conventional angiography, comparable (at least visually) to larger venous structures like the sagittal sinus in some instances.

Figure 4 illustrates the effect of delay time on the conspicuity of AVM and draining vessels, with delay times varying from 200 to 1500 ms. As expected, the mean intensity of labeled water averaged over the brain and AVM appears relatively constant (after correction for T1 relaxation). The mean intensity of labeled water in a region of interest placed over middle cerebral artery (MCA) branches decreases until it stabilizes at 800 ms and above. In contrast, the mean intensity of label in the AVM region of interest peaks between 400–800 ms and then decreases with longer delay times. Label in the sagittal sinus appears at the earliest delay times and steadily increases to the longest delay of 1500 ms, so this likely represents a combination of rapid transit and a range of slower transit times as label moves through abnormal vessels in the AVM and adjacent large draining vessels. Mean intensity of label in a

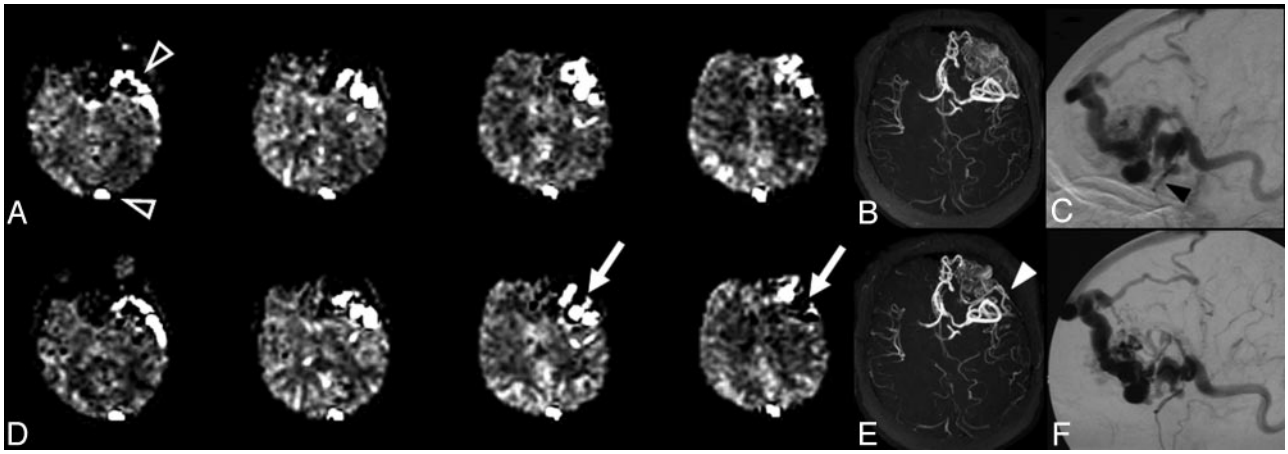

Fig 2. AVM before (top) and 2 days after (bottom) partial embolization (patient 1). CASL ΔM images (*A, D*) show decrease in AV shunt (*arrows, D*), estimated decrease from 23% to 20%. Superficial venous drainage is identified, including the superior sagittal sinus and sphenobasal sinus on both studies (*open arrowheads, A*). Of interest, despite intense signal intensity in the sphenobasal sinus, this corresponds to a relatively small venous structure on DSA (*black arrowhead, C*). DSA lateral projections (*C, F*) and 3D TOF MRA collapsed maximum intensity projection images (*B, E*) confirm decreased flow in a portion of AVM, especially the posterior-superior portion (*white arrowhead, E*).

region of interest over the sagittal sinus increases from 200–1500 ms, suggesting continued draining of labeled blood from the AVM into the superficial venous system. In this and the cases shown in Figs 1 and 2, draining venous structures appeared to be the dominant location of labeled blood corresponding to AVM and shunt. No attempt was made to separate nidus from draining vessels in this study.

No significant differences were detected in CBF measured in the basal ganglia, thalamus, or white and gray matter structures in regions close to the AVM compared with mirror regions on the contralateral side on the basis of paired *t* tests (Table 2). However, Δ (contralateral-ipsilateral) values in white matter for both raw signal intensity ($R^2 = 0.70$, $P = .02$) and calculated CBF ($R^2 = 0.73$, $P = .01$) were negatively correlated with percent AV shunt in white matter near the AVM; in other words, blood flow in adjacent ipsilateral white matter increased as percent shunt increased (Fig 5). Cortical gray matter CBF Δ values were also negatively correlated with percent AV shunt, but the correlation was weak and not significant for either raw signal intensity or CBF differences. Basal ganglia Δ values showed little change in raw signal intensity or CBF with the size of the AV shunt (Fig 5), but thalamic CBF appeared to decrease ipsilaterally with percent AV shunt (positive correlation, $R^2 = 0.74$; $P = .01$). Similar results were obtained for raw signal-intensity difference in the thalamus.

Discussion

In this small group of relatively young patients, a static depiction of relative AV shunt was created on the basis of a delay of 1200 ms, chosen empirically to allow time for labeled spin times to move from larger arteries into the microvasculature and avoid excessive T1 decay. A more comprehensive evaluation could be obtained by collecting multiple datasets with different delay times or by modifying the ASL technique to measure transit time.[27] The practical utility of this effect may be as a complement to standard AVM evaluation. For example, one of the patients with AVM showed a moderately large hematoma adjacent to the AVM, but the AVM was still visible on conventional DSA and MRA. However, small AVMs may be difficult to detect with any technique in the acute setting when significant hemorrhage is present, and simply demonstrating the presence or absence of AV shunting could be beneficial. The same would apply to the detection of DAVF. For patients with cavernous angioma presenting with hemorrhage, detection of label in draining venous structures could allow distinction between this entity and small AVMs with hemorrhage. The sensitivity (and specificity) of this approach is unclear in this small sample. Other potential applications include follow-up of AVM or DAVF after embolization, surgery, and/or radiation therapy. This could be beneficial even if 1 or more DSA follow-up examinations could be deferred or avoided.

CBF measurements in deep gray matter structures (basal ganglia and thalamus) and cortical and white matter regions near the AVMs were not significantly different from the contralateral measurements in mirror regions of interest, and the values were plausible on the basis of expected CBF for these regions. Abnormalities in perfusion of structures near and distant from AVMs have been described,[28,29] with hyper- or hypoperfusion resulting. The small sample size here may limit our ability to detect true differences, and a more symptomatic population might improve chances of detecting a difference as well. Blood flow in adjacent ipsilateral white matter increased as percent shunt increased. Cortical gray matter CBF Δ values demonstrated the same effect, but correlation was weak and not significant. Thalamic CBF decreased ipsilaterally with in-

Fig 3. Susceptibility artifact resulting from the presence of embolic material, thrombus, and/or hemorrhage (patient 1). CASL source images from 4 imaging locations are shown.

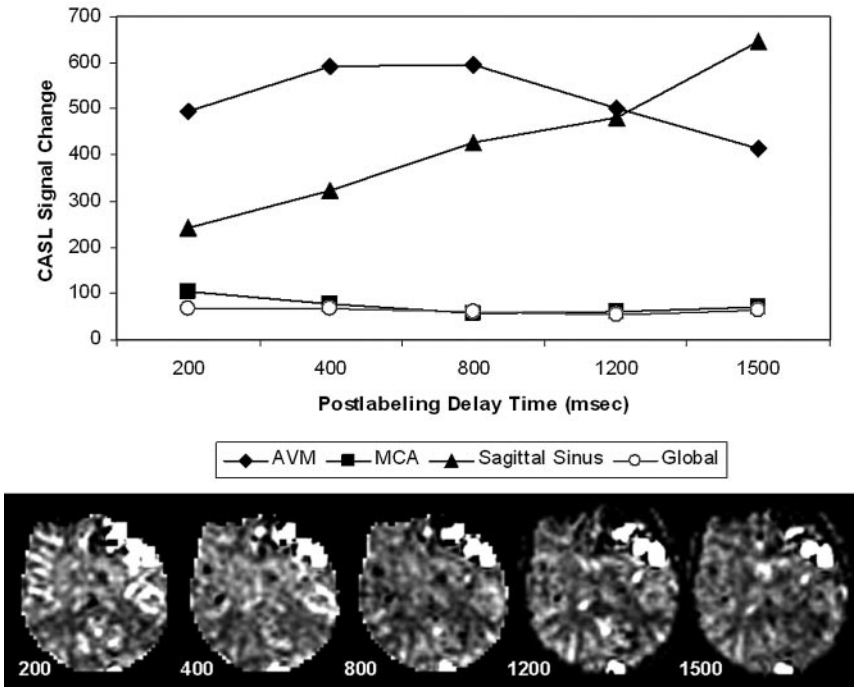

Fig 4. Multiple postlabeling delay times (200–1500 ms): effect on ASL signal intensity in the AVM (patient 1). Δ*M* (T1-corrected) measured in regions of interest for the AVM (*diamond*), sagittal sinus (*triangle*), right MCA territory (*box*), and entire brain (*circle*) at each delay is plotted (above), with Δ*M* maps from 1 imaging location at multiple delays for comparison (below). ASL signal intensity is relatively stable in global measures over the entire brain and in the MCA at longer delays as expected. Signal intensity decreases in AVM and increases in sagittal sinus as delay increases.

creasing percent AV shunt, indicating a possible steal effect from the posterior circulation. Basal ganglia measurements did not show this relationship. These relationships must be interpreted with caution in this small sample population. The AVMs studied here were primarily located in anterior circulation territories, and nearly all had a superficial drainage pattern. Cases of DAVF were not included in this analysis, and the relationship of the perfusion characteristics to patient symptoms or risk of hemorrhage was not explored. A prospective study design with a larger population and with greater variety

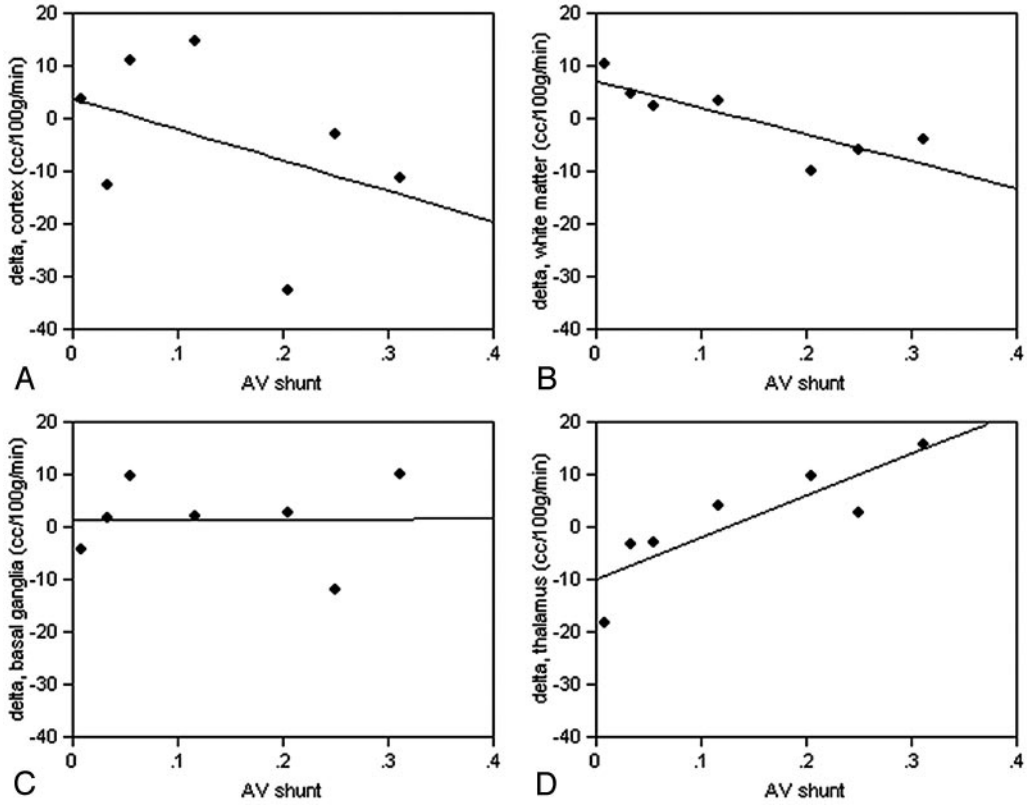

Fig 5. Regional changes in CBF compared with extent of AV shunt. Δ = contralateral − ipsilateral CBF in measured regions of interest in white matter near the AVM, the cortex near the AVM, the thalamus, and the basal ganglia. *A*, Cortical gray matter CBF Δ values are negatively but weakly correlated with percent AV shunt and are not significant. (B) Δ values in white matter ($R^2 = 0.70$, F = 11.58, $P = .02$) are negatively correlated (blood flow in adjacent ipsilateral white matter increases as percent shunt increased). Basal ganglia Δ values (*C*) show little change in CBF with the size of the AV shunt, but thalamic CBF (*D*) appears to decrease ipsilaterally as percent AV shunt increases ($R^2 = 0.74$, F = 14.19, $P = .01$).

of types and locations of vascular malformations will be required to study these relationships more completely.

Measurement of CBF by using this and similar approaches has been previously shown to be quantitative and reliable.[30-32] Transit delays present a technical challenge and can be a source of error for ASL perfusion measurements in the brain.[18] However, in the setting of AV shunt, a rapid transit abnormality is instead present where labeled blood bypasses a normal capillary bed and appears early in the draining venous system, violating assumptions for calculating CBF. AV shunt fraction calculations were thus performed by using raw signal intensity differences. In Fig 4, ΔM values plateaued at a postlabeling delay time of 400–800 ms and then decreased to the longest delay time measured (1500 ms). A steady increase in signal intensity was seen in the sagittal sinus and presumably in other draining veins not sampled; however, label completely leaving the imaging volume would affect the shunt estimation and would depend on the hemodynamics of a particular AVM.

Although calculation of absolute blood flow corresponding to an AV shunt is problematic, labeled blood supplying brain tissue elsewhere should still behave as microvascular label, and assumptions for calculating CBF in voxels corresponding to normal capillary beds should still be valid. A standard delay of 1200 ms seemed a reasonable compromise, allowing sufficient delay for label to arrive in capillaries and tissue for evaluation of CBF but retaining enough signal intensity in the AVM and draining veins for an estimate of shunt. On the other hand, draining veins appeared to dominate the signal intensity corresponding to AVMs, and the nidus was not clearly separable from draining veins. Multiple delay times may ultimately be necessary for complete evaluation, and different types and sizes of vascular malformations need to be evaluated to fully understand the relationship between nidus size, draining veins, and ASL imaging parameters. Finally, measurement error in estimates of AV shunt could not be assessed with these data, and the only method used for calculating shunt with our data was based on a simple thresholding strategy. Future studies will need to include repeated measures, and more sophisticated methods for calculating AV shunt should be explored, including alternative models.

Conclusion

ASL perfusion MR techniques can demonstrate AV shunting, providing a potentially complementary method for evaluation of AVMs as a simple means of detecting the presence of an AVM and perhaps also quantifying the extent of AV shunting. A prospective study design with a larger population, with greater variety of types and locations of vascular malformations, and with more extensive correlation with conventional angiography before and after embolization will be required for complete evaluation of this technique, and comparison with cine-phase contrast MR imaging techniques for flow quantitation may also prove useful.

References

1. Greenberg MS. *Handbook of Neurosurgery,* 4th ed. Lakeland, FL: Greenberg Graphics; 1997:871
2. Crawford PM, West CR, Chadwick DW, et al. **Arteriovenous malformations of the brain: natural history in unoperated patients.** *J Neurol Neurosurg Psychiatry* 1986;49:1–10
3. Ondra SL, Troupp H, George ED, et al. **The natural history of symptomatic arteriovenous malformations of the brain: a 24-year follow-up assessment.** *J Neurosurg* 1990;73:387–91
4. Carroll TJ, Grist TM. **Technical developments in MR angiography.** *Radiol Clin North Am* 2002;40:921–51
5. Langer DJ, Song JK, Niimi Y, et al. **Transarterial embolization of vein of Galen malformations: the use of magnetic resonance imaging noninvasive optimal vessel analysis to quantify shunt reduction—report of two cases.** *J Neurosurg* 2006;104:41–45
6. Wasserman BA, Lin W, Tarr RW, et al. **Cerebral arteriovenous malformations: flow quantitation by means of two-dimensional cardiac-gated phase-contrast MR imaging.** *Radiology* 1995;194:681–86
7. Korosec FR, Frayne R, Grist TM, et al. **Time-resolved contrast-enhanced 3D MR angiography.** *Magn Reson Med* 1996;36:345–51
8. Mistretta CA, Grist TM, Korosec FR, et al. **3D time-resolved contrast-enhanced MR DSA: advantages and tradeoffs.** *Magn Reson Med* 1998;40:571–81
9. Nael K, Michaely HJ, Villablanca P, et al. **Time-resolved contrast-enhanced magnetic resonance angiography of the head and neck at 3.0 Tesla: initial results.** *Invest Radiol* 2006;41:116–24
10. Peters DC, Korosec FR, Grist TM, et al. **Undersampled projection reconstruction applied to MR angiography.** *Magn Reson Med* 2000;43:91–101
11. Summers PE, Kollias SS, Valavanis A. **Resolution improvement in thick-slab magnetic resonance digital subtraction angiography using SENSE at 3T.** *J Magn Reson Imaging* 2004;20:662–73
12. Tsuchiya K, Aoki C, Fujikawa A, et al. **Three-dimensional MR digital subtraction angiography using parallel imaging and keyhole data sampling in cerebrovascular diseases: initial experience.** *Eur Radiol* 2004;14:1494–97
13. Buxton RB. **Quantifying CBF with arterial spin labeling.** *J Magn Reson Imaging* 2005;22:723–26
14. Chalela JA, Alsop DC, Gonzalez-Atavales JB, et al. **Magnetic resonance perfusion imaging in acute ischemic stroke using continuous arterial spin labeling.** *Stroke* 2000;31:680–87
15. Parkes LM, Tofts PS. **Improved accuracy of human cerebral blood perfusion measurements using arterial spin labeling: accounting for capillary water permeability.** *Magn Reson Med* 2002;48:27–41
16. St Lawrence KS, Frank JA, McLaughlin AC. **Effect of restricted water exchange on cerebral blood flow values calculated with arterial spin tagging: a theoretical investigation.** *Magn Reson Med* 2000;44:440–49
17. Alsop DC. **Perfusion MR Imaging.** In: Atlas SW, ed. *Magnetic Resonance Imaging of the Brain and Spine,* 3rd ed. Philadelphia: Lippincott Williams and Wilkins; 2002:215–38.
18. Wong EC. **Quantifying CBF with pulsed ASL: technical and pulse sequence factors.** *J Magn Reson Imaging* 2005;22:727–31
19. Dixon WT, Du LN, Faul DD, et al. **Projection angiograms of blood labeled by adiabatic fast passage.** *Magn Reson Med* 1986;3:454–62
20. Nishimura DG, Macovski A, Pauly JM. **Considerations of magnetic resonance angiography by selective inversion recovery.** *Magn Reson Med* 1988;7:472–84
21. Nishimura DG, Macovski A, Pauly JM, et al. **MR angiography by selective inversion recovery.** *Magn Reson Med* 1987;4:193–202
22. Essig M, Engenhart R, Knopp MV, et al. **Cerebral arteriovenous malformations: improved nidus demarcation by means of dynamic tagging MR-angiography.** *Magn Reson Imaging* 1996;14:227–33
23. Lu H, Clingman C, Golay X, et al. **Determining the longitudinal relaxation time (T1) of blood at 3.0 Tesla.** *Magn Reson Med* 2004;52:679–82
24. Alsop D, Detre J. **Multisection cerebral blood flow MR imaging with continuous arterial spin labeling.** *Radiology* 1998;208:410–16
25. Wang J, Zhang Y, Wolf RL, et al. **Amplitude-modulated continuous arterial spin-labeling 3.0-T perfusion MR imaging with a single coil: feasibility study.** *Radiology* 2005;235:218–28
26. Wolf RL, Wang J, Wang S, et al. **Grading of CNS neoplasms using continuous arterial spin labeled perfusion MR imaging at 3 Tesla.** *J Magn Reson Imaging* 2005;22:475–82
27. Hendrikse J, van Osch MJ, Rutgers DR, et al. **Internal carotid artery occlusion assessed at pulsed arterial spin-labeling perfusion MR imaging at multiple delay times.** *Radiology* 2004;233:899–904
28. Ducreux D, Buvat I, Meder JF, et al. **Perfusion-weighted MR imaging studies in brain hypervascular diseases: comparison of arterial input function extractions for perfusion measurement.** *AJNR Am J Neuroradiol* 2006;27:1059–69
29. Guo WY, Wu YT, Wu HM, et al. **Toward normal perfusion after radiosurgery: perfusion MR imaging with independent component analysis of brain arteriovenous malformations.** *AJNR Am J Neuroradiol* 2004;25:1636–44
30. Floyd TF, Ratcliffe SJ, Wang J, et al. **Precision of the CASL-perfusion MRI technique for the measurement of cerebral blood flow in whole brain and vascular territories.** *J Magn Reson Imaging* 2003;18:649–55
31. Parkes LM, Rashid W, Chard DT, et al. **Normal cerebral perfusion measurements using arterial spin labeling: reproducibility, stability, and age and gender effects.** *Magn Reson Med* 2004;51:736–43
32. Ye FQ, Berman KF, Ellmore T, et al. **H(2)(15)O PET validation of steady-state arterial spin tagging cerebral blood flow measurements in humans.** *Magn Reson Med* 2000;44:450–56